Toxic PR_n poly-dipeptides encoded by the *C9orf72* repeat expansion block nuclear import and export

Kevin Y. Shi[a,1], Eiichiro Mori[a,1], Zehra F. Nizami[b], Yi Lin[a], Masato Kato[a], Siheng Xiang[a], Leeju C. Wu[a], Ming Ding[a], Yonghao Yu[a], Joseph G. Gall[b], and Steven L. McKnight[a,2]

[a]Department of Biochemistry, University of Texas Southwestern Medical Center, Dallas, TX 75390 and [b]Department of Embryology, Carnegie Institution for Science, Baltimore, MD 21218

Contributed by Steven L. McKnight, December 9, 2016 (sent for review October 4, 2016; reviewed by Clodagh C. O'Shea and J. Paul Taylor)

The toxic proline:arginine (PR_n) poly-dipeptide encoded by the $(GGGGCC)_n$ repeat expansion in the *C9orf72* form of heritable amyotrophic lateral sclerosis (ALS) binds to the central channel of the nuclear pore and inhibits the movement of macromolecules into and out of the nucleus. The PR_n poly-dipeptide binds to polymeric forms of the phenylalanine:glycine (FG) repeat domain, which is shared by several proteins of the nuclear pore complex, including those in the central channel. A method of chemical footprinting was used to characterize labile, cross-β polymers formed from the FG domain of the Nup54 protein. Mutations within the footprinted region of Nup54 polymers blocked both polymerization and binding by the PR_n poly-dipeptide. The aliphatic alcohol 1,6-hexanediol melted FG domain polymers in vitro and reversed PR_n-mediated enhancement of the nuclear pore permeability barrier. These data suggest that toxicity of the PR_n poly-dipeptide results in part from its ability to lock the FG repeats of nuclear pore proteins in the polymerized state. Our study offers a mechanistic interpretation of PR_n poly-dipeptide toxicity in the context of a prominent form of ALS.

C9orf72 repeat expansion | PR_n poly-dipeptide | nuclear pore | FG domain | labile cross-β polymers

Expansion of the $(GGGGCC)_n$ hexanucleotide repeat within the first intron of the *C9orf72* gene is the genetic alteration leading to the most prevalent heritable form of amyotrophic lateral sclerosis (ALS) (1, 2). The expanded repeat is transcribed from both sense and antisense strands relative to the *C9orf72* gene (3–5), and both transcripts are translated in an ATG-independent manner to yield five distinct poly-dipeptides (4, 6). Expression of either the glycine:arginine (GR_n) or proline:arginine (PR_n) poly-dipeptide in *Drosophila melanogaster* leads to toxicity (7), and synthetic forms of both peptides are toxic to mammalian cells (8).

Three previous reports have led to the common finding that toxicity of RNA transcripts of the hexanucleotide expansion, or of poly-dipeptides encoded by the expansion, can be rescued by altered expression of specific cellular proteins (9–11). An unbiased screen of *D. melanogaster* genes that, when deleted, either exacerbate or mitigate *C9orf72* toxicity led to the discovery of proteins involved in both RNA biogenesis and nuclear transport (9). Similar findings were reported for the underexpression or overexpression of yeast proteins that modulate toxicity of the PR_n poly-dipeptide (11).

More recently, two independent proteomic approaches have been used to examine the distribution of intracellular proteins targeted by the toxic PR_n and GR_n poly-dipeptides (12, 13). Prominent among the intracellular targets of these toxic poly-dipeptides are nucleoporin proteins, including those composed of phenylalanine:glycine (FG) repeats (Nup54, Nup98, Nup153, and Nup214).

Here we report that the toxic PR_n poly-dipeptide binds to the central channel of the nuclear pore and inhibits the transport of macromolecules into and out of the nucleus. The PR_n poly-dipeptide also binds to polymeric forms of FG repeats derived from two proteins of the nuclear pore complex (Nup54 and Nup98). These findings provide a mechanistic understanding of how the PR_n poly-dipeptide might poison a fundamental aspect of cell function in the context of ALS.

Results

Toxic PR_n Poly-Dipeptide Binds the Central Channel of Nuclear Pores and Impedes the Import and Export of Macromolecules. A green fluorescent protein (GFP) linked to 20 repeats of the PR_n poly-dipeptide was applied to Triton X-100–permeabilized mammalian cells. This GFP:PR_{20} fusion protein bound to the nuclear periphery in a punctate pattern. Colocalization of the GFP:PR_{20} fusion protein with labeled wheat germ agglutinin (WGA) suggested that it might be binding to nuclear pores (Fig. S1).

To test this hypothesis, we examined hand-isolated giant nuclei from *Xenopus laevis* oocytes. A peptide composed of 20 repeats of PR_{20} was synthesized with a fluorescein isothiocynate (FITC) or Atto-647 dye attached to the amino terminus. In these experiments, a large fragment of the nuclear envelope was attached to a coverslip and viewed face-on by super-resolution microscopy. Both PR_{20} and WGA bound to the nuclear envelope in a punctate pattern (Fig. 1). Some envelopes treated with PR_{20} or WGA were immunostained with an antibody against gp210, a protein known to occupy the periphery of the nuclear pore complex (14). In both cases, a gp210 label surrounded the PR_{20} or WGA label (Fig. 1). We conclude that PR_{20}, like WGA, binds to the central channel of the nuclear pore complex.

Significance

A hexanucleotide repeat expansion in the first intron of the *C9orf72* gene represents the most prominent form of heritable amyotrophic lateral sclerosis. Bidirectional transcription and ATG-independent translation of the expanded $(GGGGCC)_n$ repeat specifies the production of toxic glycine:arginine (GR_n) and proline:arginine (PR_n) poly-dipeptides. The present study provides evidence that the PR_n poly-dipeptide binds directly to the central channel of nuclear pores, causing inhibition of both the import and export of macromolecules to and from the nucleus. Nuclear pore binding is shown to be mediated via direct interaction between the toxic PR_n poly-dipeptide and polymeric forms of nuclear pore proteins enriched in phenylalanine:glycine repeats.

Author contributions: K.Y.S., E.M., Z.F.N., J.G.G., and S.L.M. designed research; K.Y.S., E.M., Z.F.N., Y.L., M.K., S.X., L.C.W., M.D., and Y.Y. performed research; K.Y.S., E.M., Z.F.N., J.G.G., and S.L.M. analyzed data; and K.Y.S., E.M., J.G.G., and S.L.M. wrote the paper.

Reviewers: C.C.O., Salk Institute; and J.P.T., St. Jude Children's Medical Hospital.

The authors declare no conflict of interest.

Freely available online through the PNAS open access option.

See Commentary on page 1445.

[1]K.Y.S. and E.M. contributed equally to this work.

[2]To whom correspondence should be addressed. Email: Steven.McKnight@UTSouthwestern.edu.

This article contains supporting information online at www.pnas.org/lookup/suppl/doi:10.1073/pnas.1620293114/-/DCSupplemental.

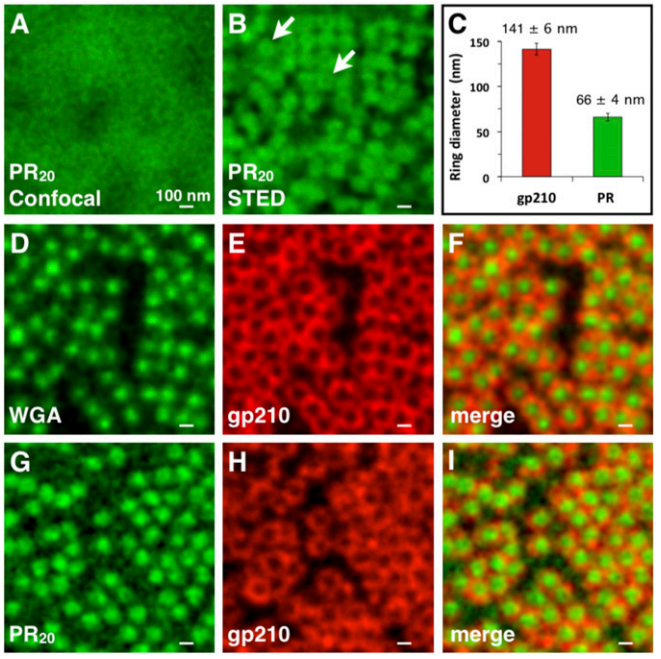

Fig. 1. STED images of PR_{20} binding to nuclear pores of *X. laevis* oocyte germinal vessicles. (*A*) FITC-labeled PR_{20} peptide (green) bound to the nuclear envelope in a punctate pattern, but individual pores were not resolvable by confocal microscopic imaging. (*B*) The same field as in *A* viewed by STED microscopy. Individual nuclear pores were thus resolved. In some pores, PR_{20} peptide binding appeared annular (arrows). (*C*) Graph comparing sizes of 250 annuli labeled with an antibody against the nucleoporin gp210 or with the PR_{20} peptide, with dimensions similar to those described by Löschberger et al. (15) and Göttfert et al. (40). (*D–F*) WGA-Alexa Fluor 555 (pseudocolored green) labeled the central channel of nuclear pores, whereas antibody against nucleoporin gp210 (red) labeled the pore periphery in an annular pattern. (*G–I*) Atto 647-PR_{20} (pseudocolored green) labeled the central channel, whereas an antibody against nucleoporin gp210 (red) labeled the periphery of nuclear pores.

A more detailed analysis of the localization of the dye-labeled PR_{20} poly-dipeptide on *X. laevis* nuclear pores is presented in Fig. 2. These data reveal an annular pattern of peptide binding corresponding to a ring with an outside diameter of 68 nm. This observation closely corresponds to the physical dimensions of nuclear pores as deduced by a previous independent super-resolution microscopy study (15), which used dye-labeled WGA to visualize the central channel of nuclear pores and was interpreted to reflect WGA staining of nucleoporin proteins rich in FG repeats. FG domains are heavily glycosylated by *O*-linked β-*N*-acetylglucosamine, thus accounting for avid binding by the WGA lectin probe (16). Given the similarity in WGA and PR_{20} staining patterns (Fig. 1), it is possible that the PR_{20} poly-dipeptide might also bind to the FG domains of nucleoporin proteins located within the central channel of nuclear pores.

Having observed PR_{20} binding to the nuclear pore complex, we next tested whether cells exposed to the peptide might show changes in the transport of macromolecules across the nuclear envelope. We examined export by comparing the accumulation of $polyA^+$ RNA in nuclei of control U2OS cells with that in nuclei of cells exposed to the synthetic PR_{20} peptide. In situ hybridization of cells treated with the PR_{20} peptide showed an increase of $polyA^+$ RNA in nuclear foci. This finding may be attributable to deficits in the export of macromolecules from the nucleus (Fig. 3*A*), and also may be consistent with PR_{20}-mediated impediments to pre-mRNA splicing (8). We also examined nuclear import by comparing the localization of a GFP protein tagged with both nuclear localization and export signals in control U2OS cells and in cells treated with the PR_{20} peptide. The peptide impeded the nuclear import of GFP in a dose-dependent manner (Fig. 3*B*).

To further test the effect of PR_{20} on nuclear import, we permeabilized HeLa cells with digitonin and exposed them to HeLa cytosol and fluorescent-tagged bovine serum albumin (BSA) conjugated to a nuclear localization peptide. Microscopic analysis of control cells revealed exclusive nuclear localization of the fluorescent-tagged BSA (Fig. 3*C*). The same experiment performed in the presence of increasing doses of the PR_{20} peptide resulted in graded exclusion of BSA from the nuclei (Fig. 3*D*). No impediment to the transport of BSA was observed when permeabilized HeLa cells were exposed to either 2.5 μM or 5 μM concentrations of synthetic PG_{20} or PA_{20} poly-dipeptides (Fig. S2). Thus, among the three poly-dipeptides encoded by the *C9orf72* repeat expansion analyzed in this study, only the PR_{20} variant was able to impede nuclear pore function.

Toxic PR_n Poly-Dipeptide Binds to Polymeric Forms of the FG Domains of Nup54 and Nup98. FG repeats are found in several proteins of the nuclear pore complex, including those in the central channel, and are believed to form the major filtration barrier of the nuclear pore (17–20). WGA binds to glycosylated FG domains, thereby inhibiting nuclear transport (16). The similar patterns of PR_{20} and WGA staining of nuclear pores (Fig. 1) suggests that the toxic PR_n poly-dipeptide might bind to FG domains of nuclear pore proteins as well.

When expressed in *Escherichia coli*, purified and incubated under physiological salt concentrations at neutral pH, the low-complexity (LC) domains of many RNA-binding proteins polymerize into labile, cross-β fibers (21). Previous studies of nucleoporin

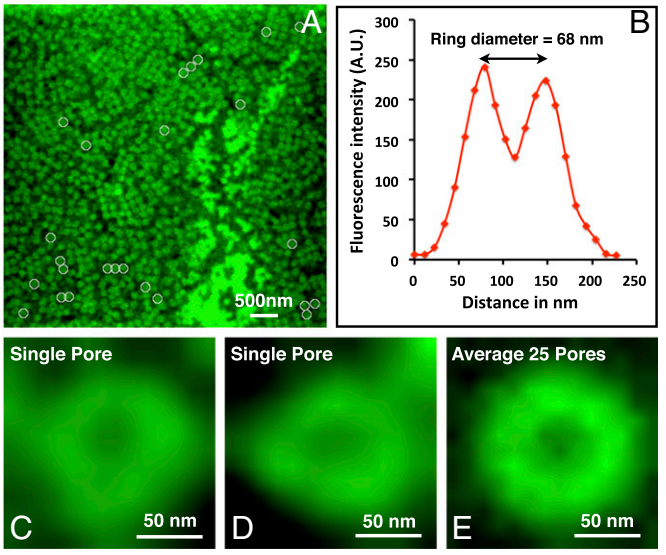

Fig. 2. Ring diameter of PR_{20} poly-dipetide localization is consistent with the diameter of the central channel of the nuclear pore complex. (*A*) A portion of unfixed *X. laevis* oocyte nuclear envelope stained with Atto647N-PR_{20} peptide and imaged with the STED 775-nm laser. Only single stained envelopes were used for quantification, because these offered the highest resolution. (*B*) An average line profile plot of the image in *E* was generated in FIJI (ImageJ) and exported to MS Excel. The line was placed diagonally across the region of interest and rotated eight times using a custom macro script. (*C* and *D*) Magnification of two example single pores from the 25 pores selected for analysis shown by the white circles in *A*. (*E*) The 25 single pores selected in *A* were aligned into a stack and then averaged in FIJI using a custom macro script. Ten such "average" pores from 10 different images were used to determine the average ring diameter shown in Fig. 1*C*. Pores were hand-selected to ensure that the analysis was conducted only on pores with a visible ring structure.

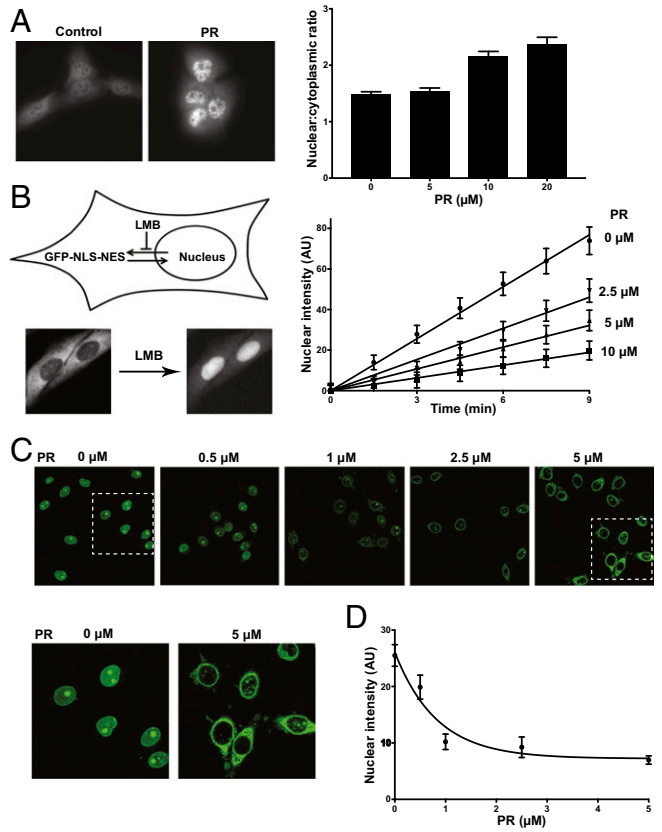

Fig. 3. PR_{20} poly-dipeptides impede the nuclear export and import of macromolecules. (*A*) U2OS cells were exposed to 2.5, 5, or 10 μM concentrations of a synthetic peptide containing 20 repeats of the PR poly-dipeptide (PR_{20}). Then, 8 h later, the cells were fixed and probed for polyA+ RNA by in situ hybridization. Cells exposed to PR_{20} retained polyA+ RNA in the nucleus in a speckled pattern. Quantitation of >50 cells per dose (*Right*) shows the relative intensity of the in situ hybridization signal in the cytoplasmic and nuclear compartments as a function of PR_{20} dose. (*B*) Diagram of a U2OS cell stably expressing GFP fused to both nuclear import and export signals. (*Left*) Under control conditions, most of the GFP accumulates in the cytoplasm. (*Right*) Leptomycin B (LMB) inhibits nuclear export, causing GFP to accumulate in the nucleus. The concentration of GFP in the nucleus, measured by fluorescence intensity, rose linearly as a function of time after the addition of LMB (control). Preincubating cells with PR_{20} poly-dipeptide inhibited the accumulation of GFP in the nucleus in a dose-dependent manner (2.5–10 μM). (*C*) HeLa cells were permeabilized with digitonin and exposed to concentrated HeLa cytoplasm along with fluorescein-labeled BSA coupled to a nuclear localization signal. Such cells accumulated BSA in the nucleus (control). Addition of the toxic PR_{20} poly-dipeptide prevented the nuclear import of BSA, which accumulated in the cytoplasm in a dose-dependent manner (0.5–5 μM). (*D*) Graph showing the concentration of labeled BSA in the nucleus (*y* axis) as a function of PR_{20} concentration in the medium (*x* axis).

proteins have described polymerization of FG domains into cross-β fibers (22–24). We observed similar evidence of the polymerization of recombinant proteins composed of the FG domains of the human Nup54 and Nup98 nucleoporin proteins. We used three methods to characterize these polymers: transmission electron microscopy, X-ray diffraction, and semidenaturing detergent agarose gel electrophoresis (SDD-AGE). After negative staining and visualization by electron microscopy, both Nup54 and Nup98 polymers appeared as unbranched fibers ∼10 nm wide and of indefinite length (Fig. 4*A*).

Polymers concentrated by centrifugation were buffer-exchanged into deionized water, lyophilized, and evaluated by X-ray diffraction. As shown in Fig. 4*B*, both Nup54 and Nup98 polymers yielded diffraction rings prototypical of amyloid polymers (4.7 and 10 Å, respectively). When evaluated by SDD-AGE, both polymers dissolved and migrated in the monomeric state (Fig. 4*C*). Thus, although polymers formed by the FG repeats of Nup54 and Nup98 display morphologies and X-ray diffraction patterns indistinguishable from those of highly stable, prion-like amyloids, both are markedly different in being labile to depolymerization on dilution.

We next performed a chemical footprinting assay to probe the structure of Nup54 polymers. Nup54 protein existing in either the polymeric state or the denatured state was exposed to *N*-acetylimidazole (NAI), a relatively nonspecific acetylating agent (25–27). Unlabeled protein was probed by NAI modification in the polymeric state. Protein probed in the denatured, monomeric state was isotopically labeled with ^{13}C-phenylalanine. After exposure to NAI, the samples were quenched with Tris buffer to inactivate the NAI chemical, mixed together, digested with chymotrypsin, and evaluated by stable isotope labeling by/with amino acids in cell

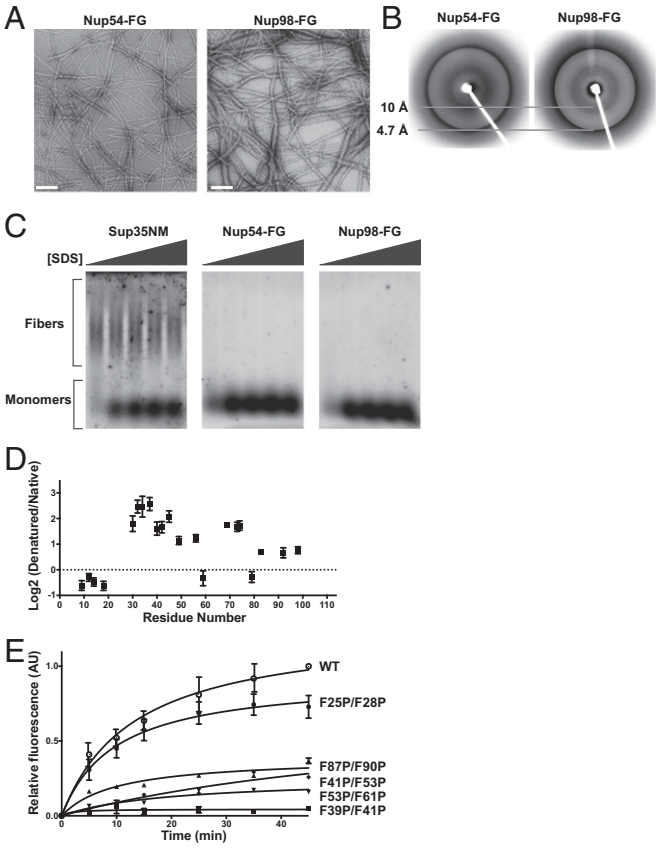

Fig. 4. Characterization of FG repeat domain polymers formed by Nup54 and Nup98. (*A*) Transmission electron micrographs of polymeric fibers of the FG domains of Nup54 and Nup98 negatively stained with uranyl acetate. (Scale bar: 200 nm.) (*B*) X-ray diffraction patterns of lyophilized Nup54 and Nup98 FG domain polymers. (*C*) SDD-AGE of amyloid polymers formed by yeast Sup35NM, Nup54 FG domain, or Nup98 FG domain. Incubation with increasing amounts of SDS did not substantially affect ySup35NM aggregates. Both Nup54 and Nup98 fibers were fully depolymerized under similar conditions. (*D*) Chemical footprinting of Nup54 fibers using the acetylation reagent NAI, as analyzed by SILAC mass spectrometry. The reactivity of specific residues in Nup54 to NAI was compared in the fully polymerized state and the denatured state. The degree of protection from acetylation on polymerization is reflected by the ratio of acetylation in denatured/native conditions (*y* axis). (*E*) WT or phenylalanine-to-proline double-mutant Nup54 monomers were incubated with WT Nup54 polymer seeds. An increase in the fluorescence of thioflavin-T (*y* axis) as a function of time (*x* axis) reflects seeded polymerization of Nup54 monomers.

culture (SILAC) mass spectrometry. As first described by Xiang et al. (25), the difference map in NAI-mediated acetylation of polymeric vs. monomeric samples can yield a chemical footprint diagnostic of the polymeric state. For Nup54 polymers, we observed a chemical footprint centrally located within the FG domain (Fig. 4*D*).

We probed the functional relevance of the NAI footprint of Nup54 polymers by mutagenesis, wherein phenylalanine residues were mutated to proline. The effects of F-to-P mutations on polymerization of the Nup54 FG domain were assessed by a thioflavin-T polymerization assay (Fig. 4*E*). Polymer formation for one mutant, which changed phenylalanine residues 25 and 28 to proline, was only mildly impeded. Intermediate impediments to polymerization were observed for three of the mutants (F41/53P, F53/61P, and F87/90P), whereas complete inhibition of polymerization was observed for the double mutant that altered phenylalanine residues located at the center of the NAI footprint (the F39/41P double mutant).

We next performed tests of PR_{20} binding to Nup54 and Nup98 polymers. Fluorescent-tagged PR_{20} peptide bound the polymeric forms of both FG domains, but not to the soluble forms of the proteins (Fig. 5 *A* and *C*). Binding was competed by unlabeled PR_{20} peptide, but not by either of the PG_{20} or PA_{20} peptides (Fig. 5 *B* and *D*). No binding of the PR_{20} probe was observed for the F39/41P double mutant of Nup54 even after incubation under conditions fully adequate for polymerization of the native FG domains of Nup54 (Fig. 5*E*). Finally, Nup54 and Nup98 FG domain polymers were exposed to FITC-labeled PR_{20} peptide and visualized by fluorescence microscopy. The fluorescent peptide bound rapidly, decorating the full length of each FG domain polymer (Fig. 5*F*).

Aliphatic Alcohols Melt FG Domain Polymers and Impede Binding of the Toxic PR_n Poly-Dipeptide. Aliphatic alcohols, including 1,6-hexanediol (1,6-HD), are known to compromise the permeability barrier of the nuclear pore (28, 29). Having observed that the FG domains of the Nup54 and Nup98 nucleoporins can polymerize into labile, cross-β polymers, we then exposed the samples to either 1,6-HD or 2,5-hexanediol (2,5-HD). Polymeric fibers formed from the FG domains of Nup54 and Nup98 were effectively dissolved by 1,6-HD, but less so by 2,5-HD (Fig. 6*A*). The 1,6-HD also inhibited PR_{20} binding to the polymeric fibers to a far greater degree than achieved by 2,5-HD (Fig. 6*B*).

As shown in Fig. 6*C*, 70-kDa dextran does not normally enter the nucleus of digitonin-permeabilized HeLa cells; however, it does enter the nucleus when the buffer is supplemented with 7% 1,6-HD, but not with 2,5-HD (Fig. 6 *C* and *D*). We hypothesize that 1,6-HD compromises the permeability barrier of nuclear pores by dissolving polymeric FG domains of nucleoporins. To test this assumption, we pretreated cells with either the PR_{20} peptide or WGA (Fig. 6 *C* and *E*), both of which bind FG domains. In both cases, the ability of 1,6-HD to facilitate nuclear import of the 70-kDa dextran was impaired, suggesting that nucleoporin polymers had been stabilized.

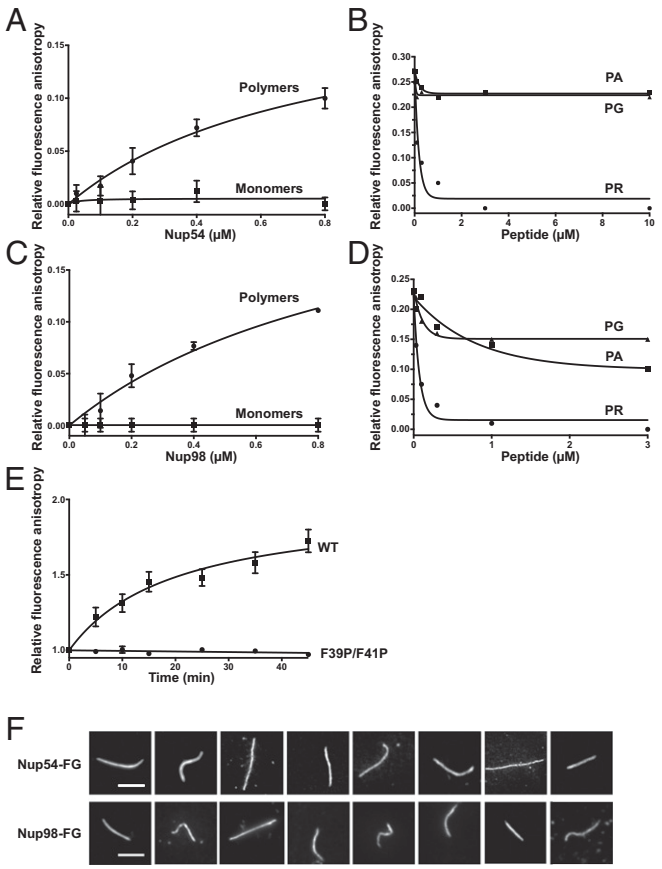

Fig. 5. PR_{20} poly-dipeptide binds to the FG repeat domain of Nup54 and Nup98. (*A*) A region encoding the FG repeats of Nup54 was expressed in bacterial cells, purified, and incubated under conditions leading to its polymerization. Monomeric and polymeric forms of the FG domain were exposed to dye-labeled PR_{20} poly-dipeptide and monitored by fluorescence polarization. Fluorescence anisotropy (*y* axis) was measured as a function of the concentration of Nup54 FG domain (*x* axis). Only the polymeric sample led to an increase in fluorescence anisotropy. (*B*) Addition of unlabeled PR_{20} peptide, but not PA_{20} or PG_{20} poly-dipeptides, displaced binding of dye-labeled PR_{20} peptide to the polymeric form of the FG domain of Nup54. (*C*) Monomeric and polymeric forms of the Nup98 FG domain were exposed to dye-labeled PR_{20} poly-dipeptide and monitored by fluorescence polarization. Fluorescence anisotropy (*y* axis) was measured as a function of the concentration of Nup98 FG domain (*x* axis). Only the polymeric sample led to an increase in fluorescence anisotropy. (*D*) The addition of unlabeled PR_{20} peptide, but not of PA_{20} or PG_{20} poly-dipeptides, displaced binding of the dye-labeled PR_{20} poly-dipeptide to Nup98 FG domain polymers. (*E*) WT or F39P/F41P mutant monomers of the Nup54 FG domain were incubated with WT polymeric seeds along with dye-labeled PR_{20}. Fluorescence anisotropy (*y* axis) was measured as a function of the time (*x* axis). Only the seeded reaction supplemented with WT monomers led to an increase in fluorescence anisotropy. (*F*) Fluorescence micrographs of dye-labeled PR_{20} poly-dipeptide bound to polymeric fibers of the FG domains of Nup54 and Nup98. (Scale bar: 20 μm.)

Discussion

Three independent studies have reported that the movement of macromolecules in and out of the nucleus is compromised in cells that carry the hexanucleotide repeat expansion $(GGGGCC)_n$ in the first intron of the *C9orf72* gene (9–11). Modifiers of this toxicity include genes encoding nucleolar proteins, heterogeneous nuclear ribonucleoproteins, and components of the nuclear pore complex (9, 11). Toxicity related to the $(GGGGCC)_n$ expansion has been variously attributed to functional disruption of the *C9orf72* gene itself (1, 2), to deleterious effects of either the sense or antisense transcript of the repeats (3, 5), and to repeat-associated non-ATG (RAN) translation products of the transcripts (4, 6). Of the five poly-dipeptides encoded by the sense and antisense transcripts of the $(GGGGCC)_n$ expansion, the arginine-rich GR_n and PR_n poly-dipeptides have been reported to exert significant toxicity (7, 8).

More recently, two independent proteomic studies identified hundreds of intracellular targets of the toxic GR_n and PR_n poly-dipeptides (12, 13). Both studies found a wide range of RNA-binding proteins, intermediate filament proteins, constituents of intracellular puncta not surrounded by investing membranes, and nuclear pore proteins as targets of the toxic poly-dipeptides. Common among many of these intracellular targets is the presence of intrinsically disordered or LC domains, which have been shown to be both necessary and sufficient for binding of the PR_n poly-dipeptide (12).

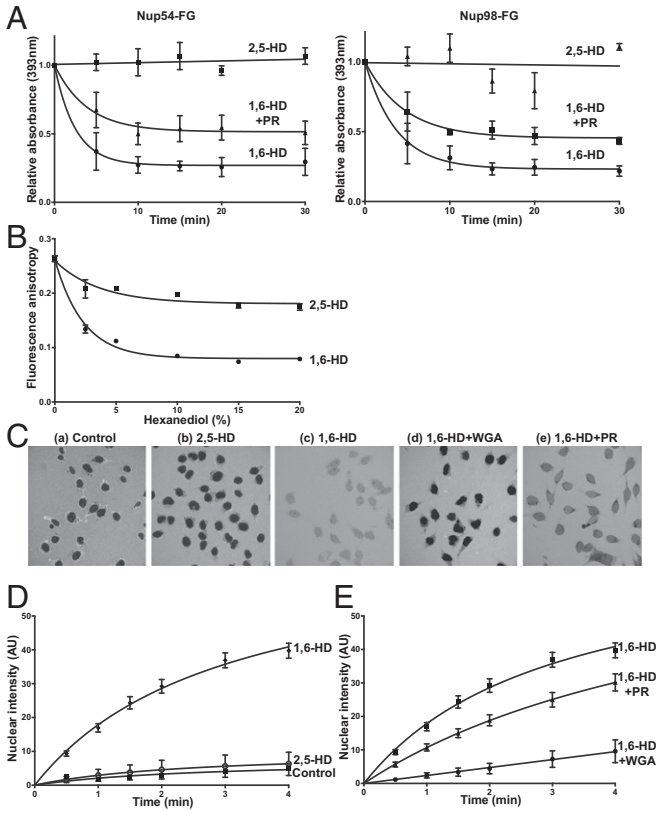

Fig. 6. Effect of aliphatic alcohols on FG domain polymers, PR_{20} binding to FG domain polymers, and nuclear partitioning of 70-kDa fluorescent dextran. (*A*) Polymeric fibers of the FG domains of Nup54 and Nup98 were exposed to 1,6-HD or 2,5-HD (15%), and polymer melting was assayed by a decrease in light scattering at 395 nm. Polymers were unaffected by 2,5-HD, but melted over a period of 30 min by 1,6-HD. Polymer melting by 1,6-HD was partially inhibited in the presence of the PR_{20} poly-dipeptide (20 μM). (*B*) Binding of dye-labeled PR_{20} poly-dipeptide to FG domain polymers was measured by fluorescence anisotropy as a function of alcohol concentration. 1,6-HD reduced PR_{20} binding more effectively than 2,5-HD. (*C*) Digitonin-permeabilized HeLa cells were exposed to 70-kDa dextran coupled to a fluorescent dye (Texas Red). (a) The fluorescent dextran was excluded from the nuclei of control cells (dark areas). (b) 2,5-HD did not affect movement of the fluorescent dextran into nuclei. (c) 1,6-HD facilitated entry of the fluorescent dextran into nuclei. (d) WGA (0.8 mg/mL) impeded 1,6-HD–mediated entry of the fluorescent dextran into nuclei. (e) PR_{20} peptide (20 μM) impeded 1,6-HD–mediated entry of the fluorescent dextran into nuclei. All images correspond to maximal uptake in 4 min. (*D*) Quantitation of the entry of fluorescent dextran into nuclei (*y* axis) as a function of time (*x* axis) after the addition of either 1,6-HD or 2,5-HD. (*E*) Quantitation of fluorescent dextran entry into nuclei (*y* axis) as a function of time (*x* axis) after the addition of 1,6-HD in the presence of the PR_{20} peptide or WGA. The curves for the effect of 1,6-HD on dextran uptake in *D* and *E* are the same data plotted in two graphs.

In the present study, we concentrated on the mechanism(s) by which the PR_n poly-dipeptide might affect the transport of macromolecules into and out of the nucleus and thus lead to the disruption of normal cellular metabolism. Specifically, we show by super-resolution microscopy that a synthetic PR_n poly-dipeptide, PR_{20}, binds to the central channel of the nuclear pore. Furthermore, PR_{20} affects both import and export of macromolecules across the nuclear envelope under several experimental conditions, as would be expected if it interferes with normal functioning of the pore complex.

Both the localization of PR_{20} and its interference with transport across the nuclear envelope suggest that proteins of the central channel might be targets of the peptide. These proteins (and other proteins of the nuclear pore complex) are rich in FG repeats, which are known to be involved in the transport process itself (20). For these reasons, we examined the interaction between PR_{20} and purified FG repeats. We found that PR_{20} did not bind to the unstructured monomeric form of FG repeats, but did bind to labile, amyloid-like FG polymers. Moreover, PR_{20} binding was reversed when the amyloid-like fibers were melted by exposure to the aliphatic alcohol 1,6-HD.

The latter properties of labile, amyloid-like fibers formed from the FG domains of the Nup54 and Nup98 proteins are reminiscent of polymers formed from LC domains derived from RNA-binding proteins (21, 30). A prominent feature of the latter category of LC domains is repetitive occurrence of the tripeptide sequence glycine/serine-tyrosine-glycine/serine (G/S-Y-G/S). We predict that LC domains enriched in either FG or G/S-Y-G/S repeats may use similar structural features to enact their respective biological function. Both types of LC domains form labile polymers that are selectively sensitive to melting by 1,6-HD (Fig. 6*A*) (12), and both bind the toxic PR_n poly-dipeptide in a polymer dependent manner (Fig. 5 *A–D*) (8, 12). We speculate that iteratively exposed epitopes along the surface of both categories of LC domain polymers allow for Velcro-like interaction with the iterative PR repeats of the toxic PR_n poly-dipeptide.

Another similarity shared by LC domains typified by either FG or G/S-Y-G/S repeats is their involvement in translocations causative of many different forms of cancer. The DNA sequences encoding FG domains of nucleoporins, or G/S-Y-G/S domains of certain RNA-binding proteins, when translocated onto sequences encoding any of various gene-specific DNA binding domains, form oncogenic fusion proteins (31–33). In both cases, the FG and G/S-Y-G/S repeats function as potent transcriptional activation domains. Studies of fused in sarcoma (FUS) and TAF15 have provided evidence that their G/S-Y-G/S repeats must be capable of polymerization to function as transcriptional activation domains (34). Whether FG domains, when translocated onto the DNA-binding domains of gene-specific transcription factors, function in a polymer-dependent manner remains to be tested.

Our results support a model in which the FG repeats of nuclear pore proteins exist in equilibrium between polymerized and unpolymerized states. The high concentration of FG domains within the central channel of nuclear pores, predicted to be in the range of 50 mM (35), favors interprotein interactions. We emphasize that the proposed cross-β segments of FG repeats within nuclear pores are likely to be very short and dynamic, perhaps composed of only a handful of polymerized subunits. By binding to polymerized FG repeats and stabilizing them, the PR_{20} peptide may shift the equilibrium toward the polymerized state, with consequent impediments to transport across the nuclear envelope. To this end, we make note of the findings of Freibaum et al. (9) showing that knockdown of the Nup98 protein suppresses the toxicity of the *C9orf72* $GGGGCC_n$ repeat expansion, perhaps by loosening the permeability barrier of the central channel of the nuclear pore.

We further show that treatment of cells with the aliphatic alcohol 1,6-HD may enhance the movement of macromolecules through nuclear pores, perhaps by shifting the equilibrium toward the unstructured state of FG repeats. The effects of the PR_{20} peptide and aliphatic alcohols represent extreme conditions; more subtle changes in the equilibrium between structured and unstructured FG repeats may regulate transport in living cells.

Materials and Methods

Peptide Synthesis. A PR_{20} peptide with an HA tag at the carboxyl terminus was synthesized by the Protein Chemistry Core at University of Texas Southwestern Medical Center. FITC and Atto-647 NHS ester were covalently conjugated to the amino terminus of glycine-PR_{20}-HA peptide and purified by reverse-phase chromatography.

Nuclear Envelope Preparation and Imaging. Nuclear envelope preparations were made from the giant oocyte nucleus of the frog *X. laevis* as described previously (36). Unfixed envelopes were treated for 20 min with 1 mg/mL nonhydrolyzable RanL43E-GTP, a kind gift from Shusheng Wang and Yixian Zheng (37). This treatment enhanced the binding of PR_{20} peptide, but was not essential. Envelopes were then incubated in either 20 μM FITC-PR_{20} or 1–5 μM Atto 647N-PR_{20} in PBS for 1 h. The resulting preparations were fixed in 4% (wt/vol) paraformaldehyde for 10 min before being mounted in ProLong Diamond mounting medium (Molecular Probes). For dual-color images, an antibody against nucleoporin gp210 was applied before the PR_{20} peptide or Alexa Fluor 555-WGA (2 μg/mL). The anti-gp210 antibody was a kind gift from Georg Krohne (14). Super-resolution images were acquired using a Leica TCS SP8 stimulated emission depletion (STED) microscope with a 1.4 NA 100× objective and 592-nm, 660-nm, and 775-nm depletion lasers.

Oligo(dT) in Situ Hybridization. To visualize polyadenylated mRNA, fluorescence in situ hybridization was carried out with a Cy3-labeled $(dT)_{40}$ probe. U2OS cells were seeded on coverslips in six-well plates, treated with PR_{20} for 8 h, and fixed with 4% (wt/vol) paraformaldehyde in PBS. The cells were permeabilized with 70% (vol/vol) ethanol at 4 °C and then incubated with the oligo(dT) probe in hybridization buffer [2× SSC, 10% (vol/vol) formamide, and 100 mg/mL dextran sulfate] at 37 °C for 4 h.

Live Cell Nuclear Import Assay. GFP that carried both a nuclear localization signal and a nuclear export signal was stably expressed in U2OS cells. At equilibrium, most GFP resides in the cytoplasm. Nuclear export was blocked with leptomycin B (LMB). Cells were incubated with various concentrations of PR_{20} peptides for 2 h before the addition of LMB. Cells were imaged with a DeltaVision microscope (GE Healthcare).

In Vitro Nuclear Import Assay. Based on previously established methods (38, 39), HeLa cells at near confluency were permeabilized with 0.005% digitonin (wt/vol) at room temperature for 5 min. The cells were treated with 2.5 μM RanGTP and various concentrations of PR_{20} for 30 min and then with PR_{20} alone for 30 min. Finally, unfractionated HeLa cytosol (4 mg/mL), an ATP/GTP-containing energy mixture, and BSA were added. The BSA was covalently conjugated with FITC and multiple SV40 nuclear localization signals. The reaction mixtures were incubated at room temperature for 25 min. After fixation with 4% (wt/vol) paraformaldehyde, the cells were imaged with a Leica confocal microscope.

Purification of the FG Domain of Nup54 and Nup98 and Formation of FG Fibers. The FG domain (residues 2–114) of Nup54 and the partial FG domain (residues 2–127) of Nup98 were expressed as His-tagged constructs in *E. coli* and purified by nickel nitrilotriacetic acid affinity chromatography. FG domain fibers were prepared by diluting the proteins from 6 M guanidinium chloride into gelation buffer (20 mM Hepes pH 7.4, 150 mM NaCl, 2 mM EDTA, and 15 mM β-mercaptoethanol) at a final concentration of 5 mg/mL. Fiber formation was confirmed by electron microscopy after negative staining with uranyl acetate.

X-Ray Diffraction of Nup Fibers. For X-ray diffraction, the Nup fiber samples were dialyzed twice in 1 L of Milli-Q water (EMD Millipore) for 12 h each time. The dialyzed samples were lyophilized overnight and then exposed to an X-ray beam to obtain cross-β diffraction as described previously (21).

SDD-AGE. The stability of cross-β fibers of Nup proteins was tested by SDD-AGE as described previously (21). In brief, Nup fibers and amyloid fibers of yeast Sup35NM protein were diluted in a gelation buffer at 1 mg/mL and briefly sonicated. Sonicated fibers were incubated in gelation buffer containing different concentrations of SDS (0–2%, wt/vol) at 37 °C for 15 min. The reaction mixtures were loaded onto a 1.5% (wt/vol) agarose gel to separate fibers and monomers. The agarose gel was then stained with Krypton Protein Stain (Thermo Fisher Scientific) overnight and subsequently scanned with a fluorescent scanner (Typhoon 9200; GE Healthcare) to visualize the proteins. Scanned images were analyzed with ImageJ.

***N*-Acetylimidazole Acetylation Footprinting of Nup54 Fibers.** These experiments were carried out in accordance with previously published protocols (21). Nup54 was expressed in *E. coli* and labeled with either light (^{12}C) or heavy (^{13}C) phenylalanine ($^{13}C_6$; labeled with ^{13}C on the six carbons of the phenyl ring) M9 medium. Light Nup54 was polymerized into fibers, isolated by centrifugation, and resuspended in buffer containing 20 mM Hepes pH 7.5, 150 mM NaCl, and 2 mM $MgCl_2$. Heavy Nup54 was denatured by boiling for 5 min in buffer containing 20 mM Hepes pH 7.5, 5 M guanidinium thiocyanate, 150 mM NaCl, and 2 mM $MgCl_2$. Then 100 μg of each sample was acetylated with 50 mM *N*-acetylimidazole at room temperature for 15 min. Reactions were quenched with equal volumes of 1.5 M Tris·HCl pH 8.8. Light and heavy samples were mixed and buffer exchanged by ultrafiltration to the 5 M guanidinium thiocyanate buffer. The mixture was boiled for 5 min, followed by further buffer exchange to a buffer containing 20 mM Hepes pH 7.5, 150 mM NaCl, 8 M urea, and 10 mM β-mercaptoethanol. Finally, three volumes of buffer containing 100 mM Tris·HCl pH 8.0, 10 mM $CaCl_2$, and 10 mM β-mercaptoethanol were added to the mixture. The sample was digested by chymotrypsin (1:50 wt/wt) overnight at room temperature and then analyzed by mass spectrometry.

Nup54 Fiber Polymerization Assay. Reactions were initiated by the addition of 2.5 μM Nup54 seeds to 25 μM Nup54 monomers [wild type (WT) or mutants] in buffer containing 20 mM Hepes pH 7.5, 150 mM NaCl, 2 mM EDTA, 10 mM β-mercaptoethanol, and 0.5 mM thioflavin-T. Fluorescence measurements were taken at 491 nm (460-nm excitation) using a photon-counting spectrofluorometer (PC1; ISS).

PR Binding to FG Domains by Fluorescence Anisotropy. Here 0.1 μM FITC-PR_{20} was mixed with various concentrations of either soluble or polymeric forms of the Nup54 or Nup98 FG domains. Fluorescence anisotropy of FITC-PR_{20} was measured at 521 nm (495-nm excitation) using a photon-counting spectrofluorometer (PC1; ISS). Competition binding experiments were carried out with 1.5 μM Nup54 or Nup98 fibers, 0.1 μM FITC-PR_{20}, and varying concentrations of nonfluorescent HA-PA_{20}, HA-PG_{20}, or HA-PR_{20}.

Imaging of FITC-PR_{20} Binding to Nup54 Polymers. Here 0.1 μM FITC-PR_{20} was mixed with Nup54 or Nup98 polymers and imaged with a 100× objective on a DeltaVision fluorescence microscope (GE Healthcare).

Nuclear Pore Permeability Assay. HeLa cells at near confluency were permeabilized with 0.005% digitonin (wt/vol) at room temperature for 5 min. Cells were exposed to buffer only containing 0.5 mg/mL of Texas Red-labeled 70 kDa dextran or to buffers containing an additional 7% (wt/vol) 1,6-HD or 2,5-HD. Permeabilized cells were also incubated with either 0.8 mg/mL WGA (Sigma-Aldrich) or 20 μM HA-PR_{20} before being exposed to buffer containing dextran and 7% (wt/vol) 1,6-HD. Cells were imaged with a Leica confocal microscope.

ACKNOWLEDGMENTS. We thank Drs. Shusheng Wang, Yixian Zheng, and Georg Krohne for kindly providing reagents; Drs. J. Paul Taylor and Clodagh C. O'Shea for a critical review of the manuscript; Dr. J. Paul Taylor for generous provision of the PA_{20} and PG_{20} synthetic peptides; and staff of the Live Cell Imaging, Electron Microscopy, and Protein Chemistry Cores at the University of Texas Southwestern Medical Center for technical assistance. This work was supported by the National Institutes of Health Grants U01 GM10762301 (to S.L.M.) and R01 GM33397 (to J.G.G.), and by unrestricted funding provided to S.L.M. from an anonymous donor. J.G.G. is an American Cancer Society Professor of Developmental Genetics. The content of this report is solely the responsibility of the authors and does not necessarily represent the official views of the National Institutes of Health.

1. DeJesus-Hernandez M, et al. (2011) Expanded GGGGCC hexanucleotide repeat in noncoding region of C9ORF72 causes chromosome 9p-linked FTD and ALS. *Neuron* 72(2):245–256.
2. Renton AE, et al.; ITALSGEN Consortium (2011) A hexanucleotide repeat expansion in C9ORF72 is the cause of chromosome 9p21-linked ALS-FTD. *Neuron* 72(2):257–268.
3. Lagier-Tourenne C, et al. (2013) Targeted degradation of sense and antisense C9orf72 RNA foci as therapy for ALS and frontotemporal degeneration. *Proc Natl Acad Sci USA* 110(47):E4530–E4539.
4. Zu T, et al. (2013) RAN proteins and RNA foci from antisense transcripts in C9ORF72 ALS and frontotemporal dementia. *Proc Natl Acad Sci USA* 110(51):E4968–E4977.
5. Mizielinska S, et al. (2013) C9orf72 frontotemporal lobar degeneration is characterised by frequent neuronal sense and antisense RNA foci. *Acta Neuropathol* 126(6): 845–857.
6. Mori K, et al. (2013) The C9orf72 GGGGCC repeat is translated into aggregating dipeptide-repeat proteins in FTLD/ALS. *Science* 339(6125):1335–1338.
7. Mizielinska S, et al. (2014) C9orf72 repeat expansions cause neurodegeneration in *Drosophila* through arginine-rich proteins. *Science* 345(6201):1192–1194.
8. Kwon I, et al. (2014) Poly-dipeptides encoded by the C9orf72 repeats bind nucleoli, impede RNA biogenesis, and kill cells. *Science* 345(6201):1139–1145.
9. Freibaum BD, et al. (2015) GGGGCC repeat expansion in C9orf72 compromises nucleocytoplasmic transport. *Nature* 525(7567):129–133.
10. Zhang K, et al. (2015) The C9orf72 repeat expansion disrupts nucleocytoplasmic transport. *Nature* 525(7567):56–61.
11. Jovičić A, et al. (2015) Modifiers of C9orf72 dipeptide repeat toxicity connect nucleocytoplasmic transport defects to FTD/ALS. *Nat Neurosci* 18(9):1226–1229.

12. Lin Y, et al. (2016) Toxic PR poly-dipeptides encoded by the C9orf72 repeat expansion target LC domain polymers. *Cell* 167(3):789–802 e712.
13. Lee KH, et al. (2016) C9orf72 dipeptide repeats impair the assembly, dynamics, and function of membrane-less organelles. *Cell* 167(3):774–788 e717.
14. Gajewski A, Lourim D, Krohne G (1996) An antibody against a glycosylated integral membrane protein of the *Xenopus laevis* nuclear pore complex: A tool for the study of pore complex membranes. *Eur J Cell Biol* 71(1):14–21.
15. Löschberger A, et al. (2012) Super-resolution imaging visualizes the eightfold symmetry of gp210 proteins around the nuclear pore complex and resolves the central channel with nanometer resolution. *J Cell Sci* 125(Pt 3):570–575.
16. Finlay DR, Newmeyer DD, Price TM, Forbes DJ (1987) Inhibition of in vitro nuclear transport by a lectin that binds to nuclear pores. *J Cell Biol* 104(2):189–200.
17. Strawn LA, Shen T, Shulga N, Goldfarb DS, Wente SR (2004) Minimal nuclear pore complexes define FG repeat domains essential for transport. *Nat Cell Biol* 6(3): 197–206.
18. Frey S, Görlich D (2007) A saturated FG-repeat hydrogel can reproduce the permeability properties of nuclear pore complexes. *Cell* 130(3):512–523.
19. Patel SS, Belmont BJ, Sante JM, Rexach MF (2007) Natively unfolded nucleoporins gate protein diffusion across the nuclear pore complex. *Cell* 129(1):83–96.
20. Radu A, Moore MS, Blobel G (1995) The peptide repeat domain of nucleoporin Nup98 functions as a docking site in transport across the nuclear pore complex. *Cell* 81(2): 215–222.
21. Kato M, et al. (2012) Cell-free formation of RNA granules: Low-complexity sequence domains form dynamic fibers within hydrogels. *Cell* 149(4):753–767.
22. Halfmann R, Wright JR, Alberti S, Lindquist S, Rexach M (2012) Prion formation by a yeast GLFG nucleoporin. *Prion* 6(4):391–399.
23. Ader C, et al. (2010) Amyloid-like interactions within nucleoporin FG hydrogels. *Proc Natl Acad Sci USA* 107(14):6281–6285.
24. Milles S, et al. (2013) Facilitated aggregation of FG nucleoporins under molecular crowding conditions. *EMBO Rep* 14(2):178–183.
25. Xiang S, et al. (2015) The LC domain of hnRNPA2 adopts similar conformations in hydrogel polymers, liquid-like droplets, and nuclei. *Cell* 163(4):829–839.
26. Riordan JF, Wacker WEC, Vallee BL (1965) *N*-Acetylimidazole: A reagent for determination of "free" tyrosyl residues of proteins. *Biochemistry* 4(9):1758–1765.
27. Timasheff SN, Gorbunoff MJ (1967) Conformation of proteins. *Annu Rev Biochem* 36: 13–54.
28. Ribbeck K, Görlich D (2002) The permeability barrier of nuclear pore complexes appears to operate via hydrophobic exclusion. *EMBO J* 21(11):2664–2671.
29. Shulga N, Goldfarb DS (2003) Binding dynamics of structural nucleoporins govern nuclear pore complex permeability and may mediate channel gating. *Mol Cell Biol* 23(2):534–542.
30. Han TW, et al. (2012) Cell-free formation of RNA granules: Bound RNAs identify features and components of cellular assemblies. *Cell* 149(4):768–779.
31. Xu S, Powers MA (2009) Nuclear pore proteins and cancer. *Semin Cell Dev Biol* 20(5): 620–630.
32. Kovar H (2011) Dr. Jekyll and Mr. Hyde: The two faces of the FUS/EWS/TAF15 protein family. *Sarcoma* 2011:837474.
33. Tan AY, Manley JL (2009) The TET family of proteins: Functions and roles in disease. *J Mol Cell Biol* 1(2):82–92.
34. Kwon I, et al. (2013) Phosphorylation-regulated binding of RNA polymerase II to fibrous polymers of low-complexity domains. *Cell* 155(5):1049–1060.
35. Bayliss R, et al. (1999) Interaction between NTF2- and xFxFG-containing nucleoporins is required to mediate nuclear import of RanGDP. *J Mol Biol* 293(3):579–593.
36. Gall JG (1967) Octagonal nuclear pores. *J Cell Biol* 32(2):391–399.
37. Wilde A, Zheng Y (1999) Stimulation of microtubule aster formation and spindle assembly by the small GTPase Ran. *Science* 284(5418):1359–1362.
38. Cassany A, Gerace L (2009) Reconstitution of nuclear import in permeabilized cells. *Methods Mol Biol* 464:181–205.
39. Adam SA, Marr RS, Gerace L (1990) Nuclear protein import in permeabilized mammalian cells requires soluble cytoplasmic factors. *J Cell Biol* 111(3):807–816.
40. Göttfert F, et al. (2013) Coaligned dual-channel STED nanoscopy and molecular diffusion analysis at 20-nm resolution. *Biophys J* 105(1):L01–L03.